

RESEARCH ARTICLE

10.1002/2015JA021000

Special Section:

Pulsating Aurora and Related Magnetospheric Phenomena

Key Points:

- Statistical study of auroral fragmentation through finger-like structures
- Changing magnetic field configuration could affect generation of the structures
- MHD instability or ion finite Larmor radius seems to generate these structures

Supporting Information:

- Supporting Information S1
- Animation S1
- Animation S2

Correspondence to:

A. Hashimoto,
a-hashimoto@stelab.nagoya-u.ac.jp

Citation:

Hashimoto, A., K. Shiokawa, Y. Otsuka, S.-i. Oyama, S. Nozawa, T. Hori, M. Lester, and M. G. Johnsen (2015), Statistical study of auroral fragmentation into patches, *J. Geophys. Res. Space Physics*, *120*, doi:10.1002/2015JA021000.

Received 10 JAN 2015

Accepted 14 JUL 2015

Accepted article online 18 JUL 2015

Statistical study of auroral fragmentation into patches

Ayumi Hashimoto¹, Kazuo Shiokawa¹, Yuichi Otsuka¹, Shin-ichiro Oyama¹, Satonori Nozawa¹, Tomoaki Hori¹, Mark Lester², and Magnar Gullikstad Johnsen³

¹Solar-Terrestrial Environment Laboratory, Nagoya University, Nagoya, Japan, ²Department of Physics and Astronomy, University of Leicester, Leicester, UK, ³Tromsø Geophysical Observatory, Norwegian Center for Space Weather, UiT The Arctic University of Norway, Tromsø, Norway

Abstract The study of auroral dynamics is important when considering disturbances of the magnetosphere. Shiokawa et al. (2010, 2014) reported observations of finger-like auroral structures that cause auroral fragmentation. Those structures are probably produced by macroscopic instabilities in the magnetosphere, mainly of the Rayleigh-Taylor type. However, the statistical characteristics of these structures have not yet been investigated. Here based on observations by an all-sky imager at Tromsø (magnetic latitude = 67.1°N), Norway, over three winter seasons, we statistically analyzed the occurrence conditions of 14 large-scale finger-like structures that developed from large-scale auroral regions including arcs and 6 small-scale finger-like structures that developed in auroral patches. The large-scale structures were seen from midnight to dawn local time and usually appeared at the beginning of the substorm recovery phase, near the low-latitude boundary of the auroral region. The small-scale structures were primarily seen at dawn and mainly occurred in the late recovery phase of substorms. The sizes of these large- and small-scale structures mapped in the magnetospheric equatorial plane are usually larger than the gyroradius of 10 keV protons, indicating that the finger-like structures could be caused by magnetohydrodynamic instabilities. However, the scale of small structures is only twice the gyroradius of 10 keV protons, suggesting that finite Larmor radius effects may contribute to the formation of small-scale structures. The eastward propagation velocities of the structures are −40 to +200 m/s and are comparable with those of plasma drift velocities measured by the colocating Super Dual Auroral Radar Network radar.

1. Introduction

Plasma disturbance in the magnetosphere can be projected to the ionosphere through auroral particles, which precipitate along geomagnetic field lines. Study of auroral dynamics is therefore important when considering disturbances of the magnetosphere. It is generally believed that there are two major types of aurora: discrete aurora and diffuse aurora including pulsating auroral patches (pulsating aurora being a subclass of the diffuse aurora) [Davis, 1978]. Nakamura and Oguti [1987] suggested that pulsating auroral patches are formed as a result of cold plasma irregularities in the distant magnetosphere. They also mentioned that not only drifts of auroral patches but also drifts of auroral arc fragments are likely due to magnetospheric electric fields.

Shiokawa et al. [2010] found small-scale finger-like structures developing into and out from individual auroral patches, and they suggested that these finger-like structures are caused by pressure-driven instabilities, such as ballooning or interchange instabilities. Shiokawa et al. [2014] analyzed two large-scale finger-like structures developing over the entire field of view of ground-based all-sky cameras and concluded that auroral fragmentations due to pressure-driven instabilities cause auroral patches. However, the statistical characteristics of these phenomena have not yet been investigated.

The purpose of this study is therefore to perform statistical analysis of the occurrence conditions of finger-like auroral structures that suggest pressure-driven plasma instabilities in the magnetosphere. We have obtained statistical characteristics of large- and small-scale finger-like structures, as well as their dependence on the interplanetary magnetic field (IMF), geomagnetic activities, and ionospheric plasma flows. From these parameters, we conclude that magnetohydrodynamic (MHD) instabilities caused the observed auroral fragmentation.

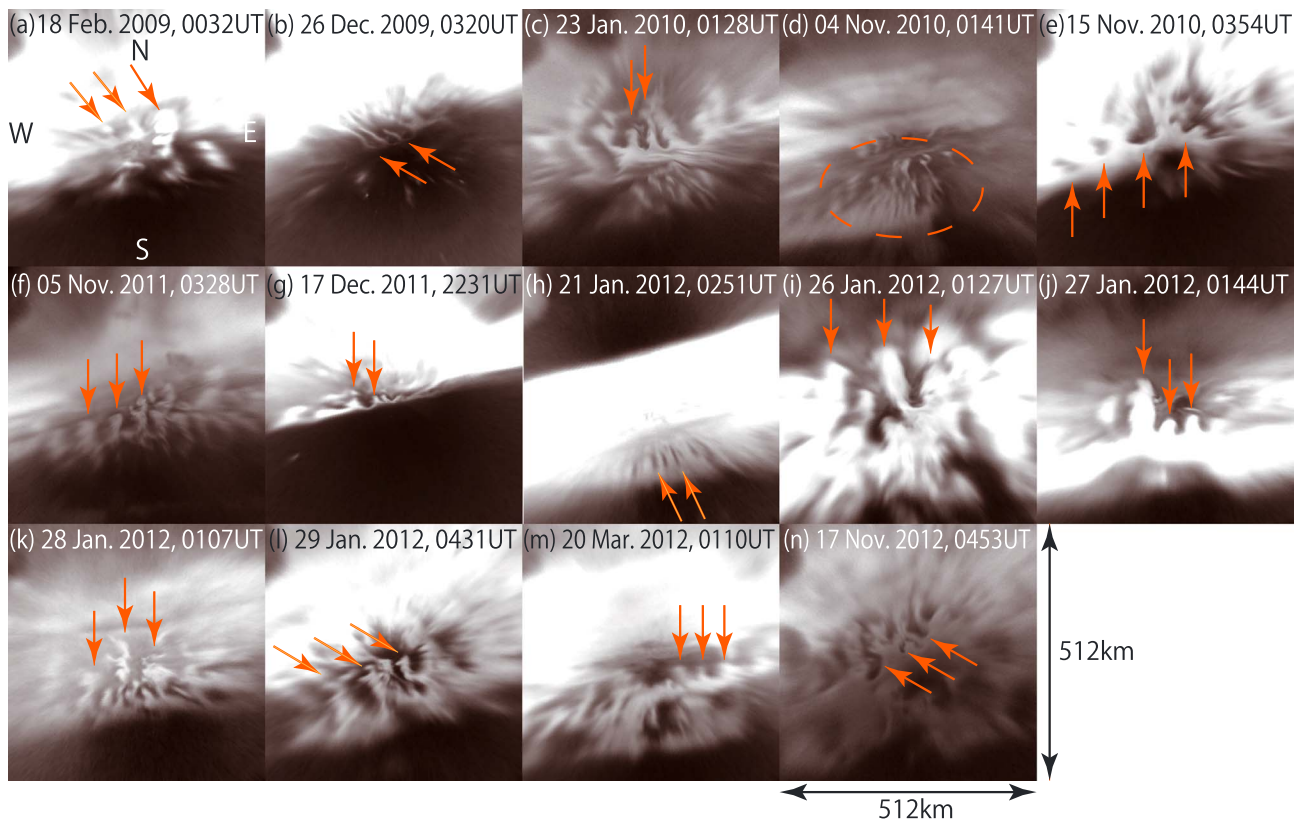


Figure 1. Auroral images of large-scale finger-like structures in geographic coordinates with an image size of 512×512 km at a wavelength of 557.7 nm. Orange arrows and circles point to large-scale finger-like structures. In this study, 14 large-scale structures were identified in a period spanning three winters.

2. Observation

We used a monochromatic cooled charge-coupled device (CCD) all-sky imager at Tromsø (69.6°N , 19.2°E , magnetic latitude (MLAT) = 67.1°N , $L = 6.6$ Re), Norway, that took 256×256 pixel images at 557.7 nm with a time resolution of 60 s (from 11 January 2009) or 95 s (from 3 November 2009). Details of the imager can be found in *Shiokawa et al.* [1999, 2009]. We also used data from the Advanced Composition Explorer (ACE) satellite, ground-based magnetograms at Tromsø, the Super Dual Auroral Radar Network (SuperDARN) radar [*Chisham et al.*, 2007] and Defense Meteorological Satellite Program (DMSP) satellites.

Shiokawa et al. [2010, 2014] described small- and large-scale finger-like auroral structures. In the present study, we provide a statistical analysis of these two types of structures. We define finger-like structures developing from large-scale (predominantly east-west) auroral regions including arcs as “large scale.” We categorize structures developing into or out from individual auroral patches as “small scale.” We used all-sky auroral images and videos to identify these structures, selecting events with more than three fingers in a structure by visual inspection. The scales of the large- and small-scale structures ranged between 20 and 90 km and between 10 and 25 km, respectively.

We considered an observation period from January 2009 to November 2012, which corresponds to about three winter seasons. The total time of clear sky was 601 h, and the time interval for which auroras reached the zenith at Tromsø was 235.5 h. We observed finger-like structures for a total of 41.5 h, representing 17.6% of the total time in which the auroras reached zenith. The large- and small-scale structures were observed for 31.5 h (13%) and 10 h (4%), respectively.

3. Observational Results for Large- and Small-Scale Structures

Figure 1 shows 512×512 km auroral images, in geographic coordinates, for all of the 14 large-scale finger-like structures that were identified in this study. The orange arrows and the circle indicate representative parts of these structures. In some cases (e.g., Figure 1l), secondary finger-like structures seemed to appear in the

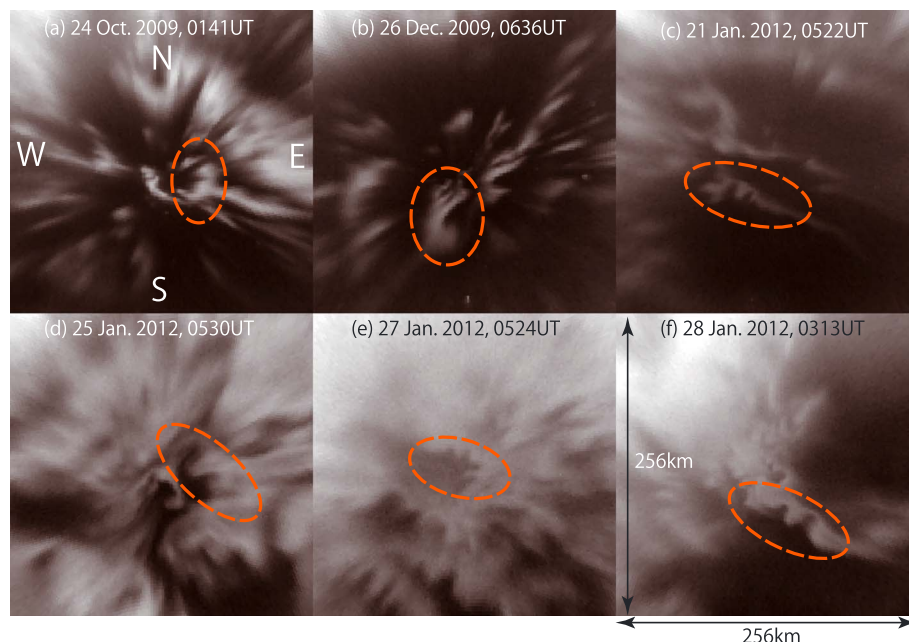


Figure 2. Auroral images of small-scale finger-like structures in geographic coordinates with an image size of 256×256 km at a wavelength of 557.7 nm. Orange circles point to small-scale finger-like structures. In this study, six small-scale structures were identified in a period spanning three winters.

large-scale structures, but we considered them as part of the large-scale finger-like structure and do not count them as small-scale finger-like structures. Of these 14 events, 13 appeared on the low-latitude side of the auroral region; no auroras were seen equatorward of these structures, except in Figure 1n. The average east-west scale of the structures (average separation between the fingers) was 48 ± 20 km for these 14 events, where the uncertainty denotes one standard deviation of the population. Both bright and dark finger-like structures developed in the north-south direction. The average and standard deviation of meridional development speeds in these 14 cases, which was measured by comparing images before and after structure development, were 80 ± 49 m/s. Animation S1 in the supporting information shows a sequence of frames illustrating the development of a large-scale finger-like structure observed on 27 January 2012, indicating that bright or dark finger-like structures started to develop meridionally at around 0140 UT and drifted eastward.

Figure 2 shows images of small-scale finger-like structures using geographic coordinates with an image size of 256 km. In these images, orange circles indicate representative parts of these small-scale structures. In

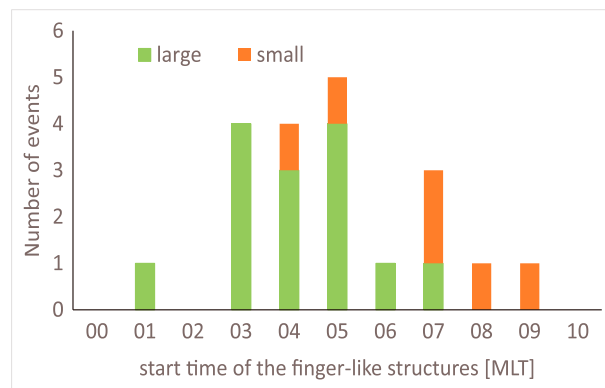


Figure 3. MLT dependence of the start time of the large- and small-scale finger-like structures.

this study, six small-scale structures developing in auroral patches were identified with an average scale of 15 ± 5 km. Either bright or black finger-like structures developed into and out from individual auroral patches. In some cases, small-scale structures developed into patches after large-scale structures had disappeared. The average and standard deviation of the development speed, which was measured by comparing images before and after structure development, were 59 ± 31 m/s. Animation S2 shows a sequence of frames observed on 26 December 2009, depicting the development of a small-scale finger-like structure as the patch becomes brighter.

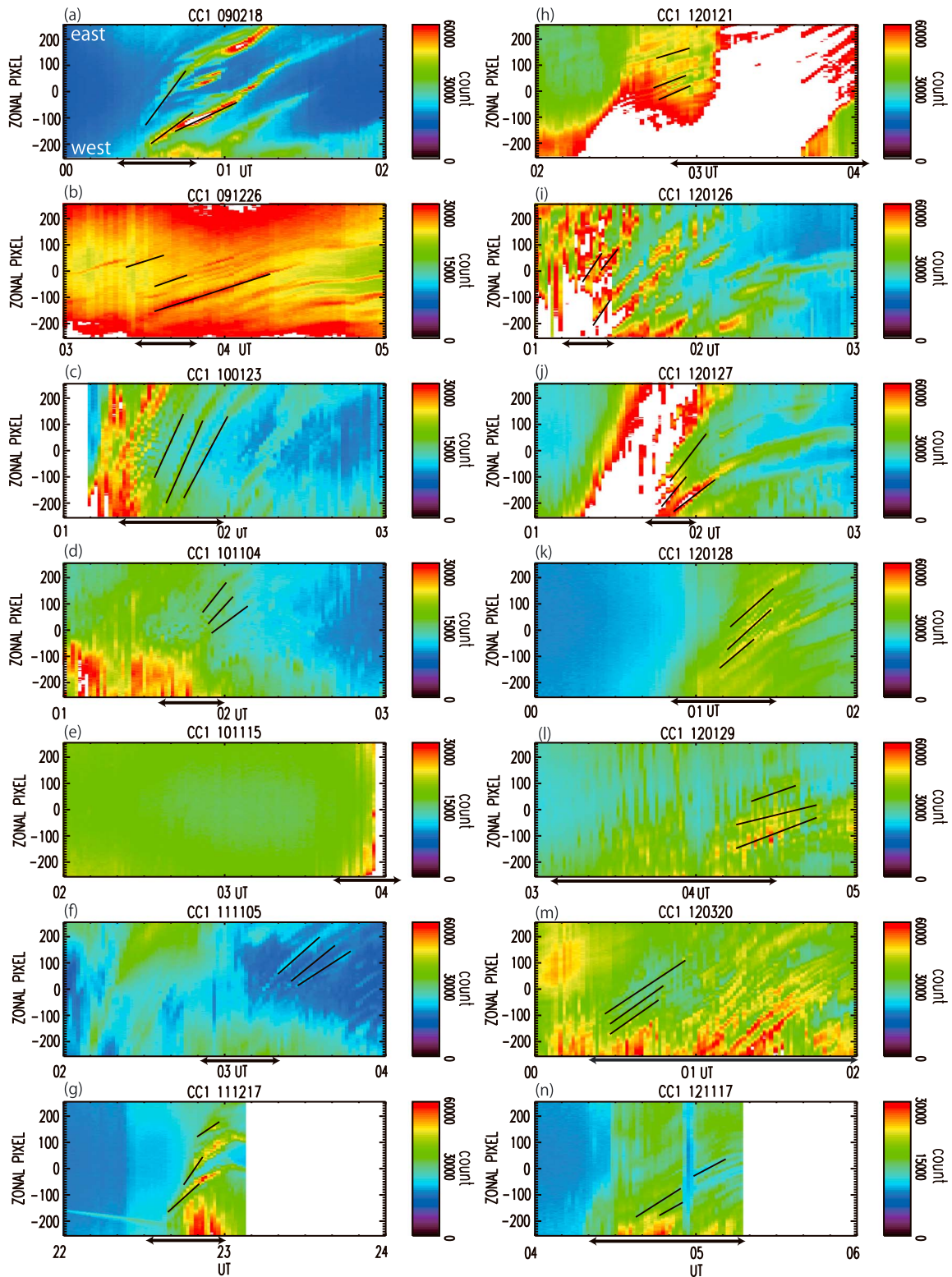


Figure 4. East-west keograms for the large-scale structures, with a horizontal axis of 2 h and a vertical axis showing distance from east to west. Horizontal black arrows under each panel show the interval of the development of finger-like structures.

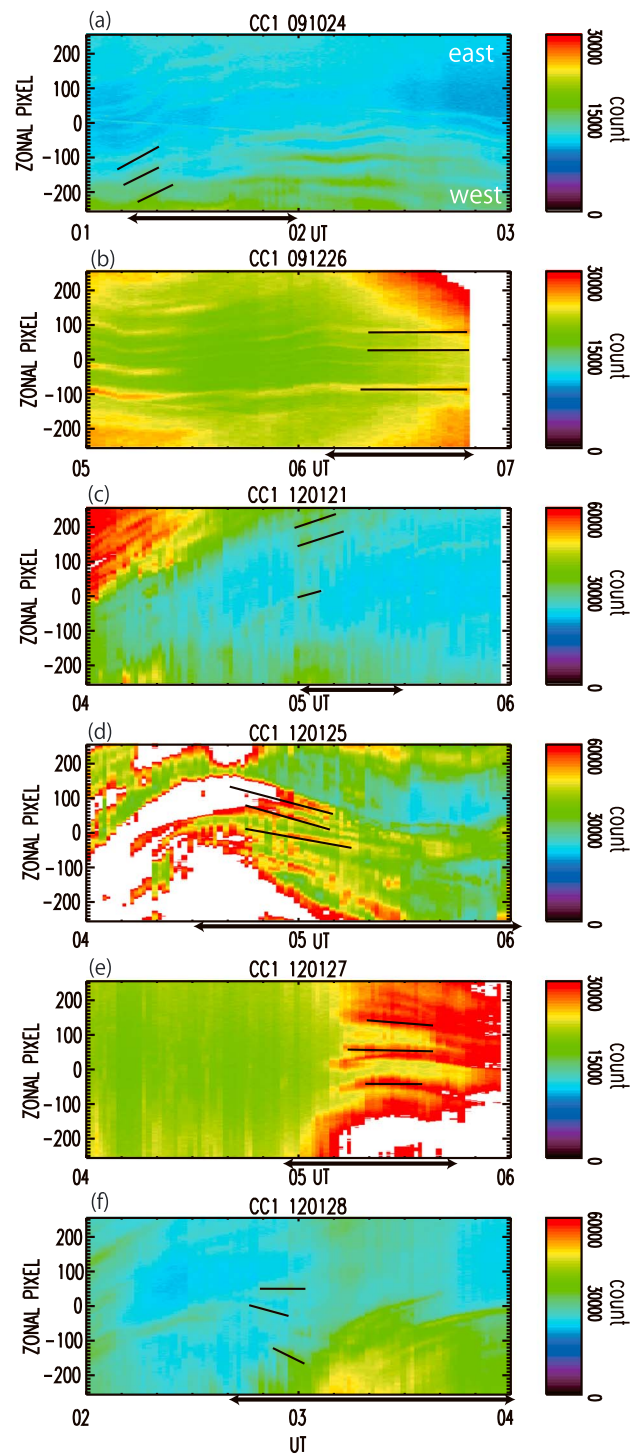


Figure 5. East-west keograms for the small-scale structures in the same format as Figure 4.

Figure 3 shows the magnetic local time (MLT) dependence of the start time of the finger-like structures. We defined the start time of the structures as the time when they start to develop in the images. The green bars show the number of large-scale finger-like structures, while the orange bars show the number of small-scale finger-like structures. MLT is calculated by adding 3.3 h to the time in UT. The large-scale structures appear between midnight and dawn, while the small-scale structures appear at dawn, after 04 MLT.

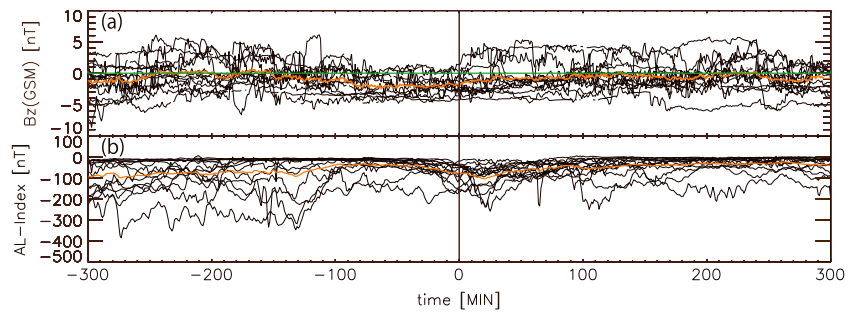


Figure 6. Superposed epoch analysis of the IMF B_z and AL index for large-scale finger-like structures. Horizontal axis is from -300 min to 300 min from the start time of the finger-like structures.

Figure 4 shows east-west keograms for large-scale finger-like structures showing the zonal cross section that passes through the zenith as a function of time. The horizontal axis covers a time span of 2 h, the vertical axis shows the distance from east (top) to west (bottom), and black arrows at the bottom of the panels show the interval of the development of finger-like structures. Black lines in the keograms are used to calculate the eastward propagation speed of these structures. The eastward propagation speeds of auroras are considered the same as those of the finger-like structures. We positioned the black lines at the time when structures were developing (shown by black arrows). However, in some cases it is difficult to determine a definitive line at a particular time. In such cases we positioned the lines as close as possible to the interval of development. In addition, because line positioning was performed manually, we have a typical uncertainty of approximately $20\text{--}50$ m/s. These panels indicate that the auroras continuously drifted eastward during development of the finger-like structures. The average and standard deviation of eastward propagation speed were 155 ± 78 m/s for the 14 events.

Figure 5 shows east-west keograms for small-scale finger-like structures in the same format as Figure 4. During development of the structures shown by the horizontal arrows below these panels, the eastward drift speeds slowed or even turned slightly westward for all six events. This finding suggests that the instability growth may be suppressed by fast plasma drift. The average and standard deviation of eastward propagation speed were 11 ± 52 m/s for the six events.

Figure 6 shows variation of the IMF B_z and AL index for large-scale finger-like structures. The horizontal axis ranges from 5 h before to 5 h after the start time of large-scale structure development. The orange line indicates the average of each parameter. In the IMF B_z data, the average line decreases below zero approximately 150 min before the start time of the structures, indicating that the IMF B_z tends to point southward at that time. The AL index decreased approximately 50 min before the start time, indicating that the westward auroral electrojet current was developed during the event.

In the same format as Figure 6, Figure 7 shows a similar superposed epoch analysis of IMF B_z and AL index for the small-scale finger-like structures. Just as in the previous case, we observe a decrease of the average IMF B_z

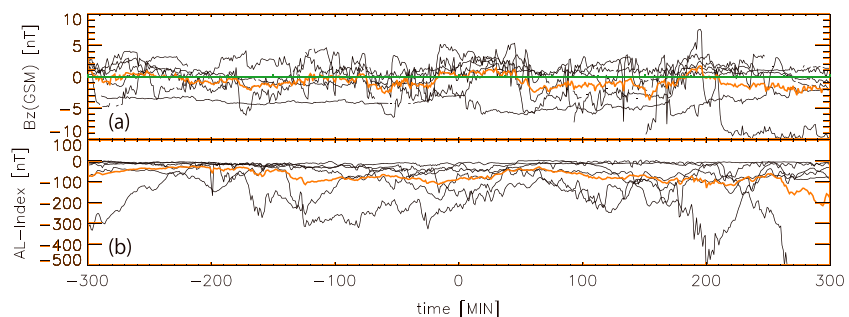


Figure 7. Superposed epoch analysis of the IMF B_z and AL index for small-scale finger-like structures in the same format as Figure 6.

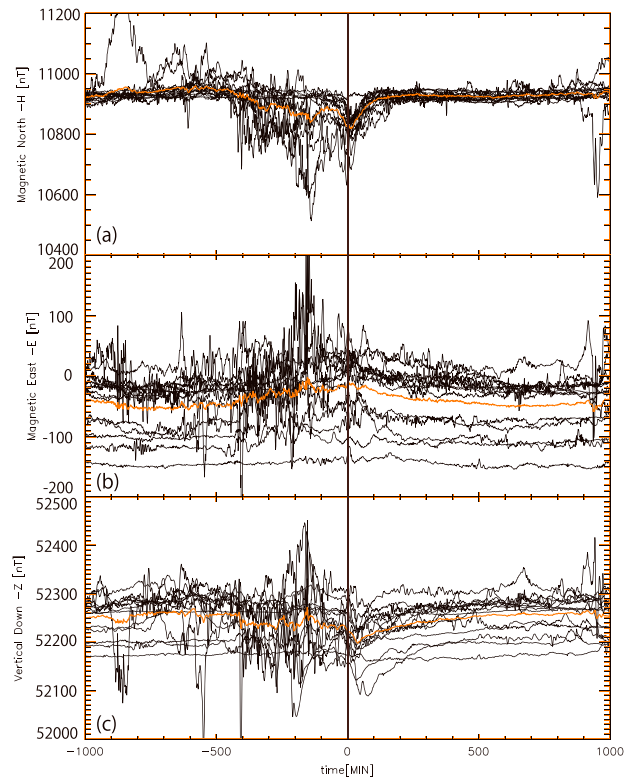


Figure 8. Magnetograms during large-scale finger-like structures at Tromsø. (a) Magnetic northward (H), (b) eastward (E), and (c) downward (Z) magnetic field variations. Horizontal axis is from -1000 min to 1000 min from the start time of the large-scale finger-like structures.

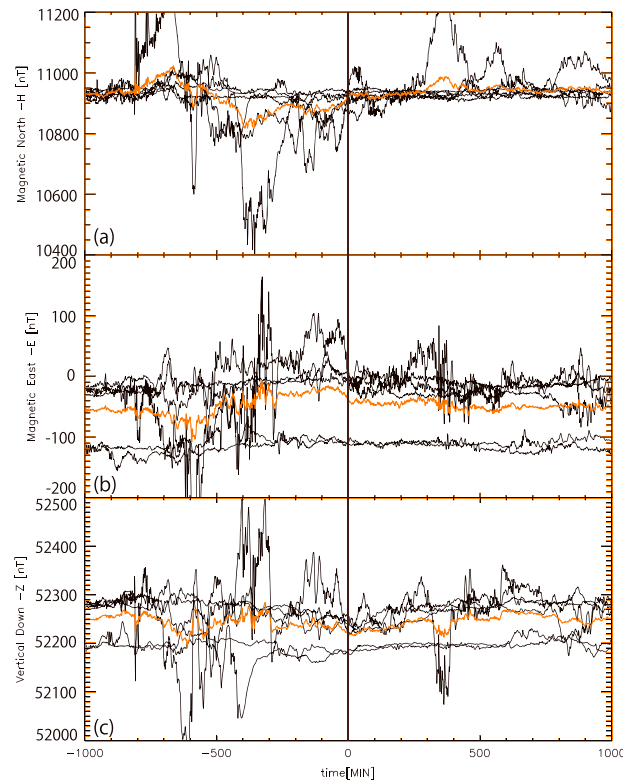


Figure 9. Magnetograms during small-scale finger-like structures at Tromsø in the same format as Figure 8.

approximately 200 min before the start time. However, unlike the large-scale structures, the decrease is less noticeable and turns northward at the start time. The AL index also decreases slightly.

Figure 8 shows a superposed epoch analysis of magnetic field variations seen at Tromsø during the observation of large-scale finger-like structures. Northward (H), eastward (E), and downward (Z) magnetic field variations are shown in Figures 8a–8c. The horizontal axis ranges from 1000 min before to 1000 min after the large-scale structures started to develop. Between the times of approximately -400 min and 0 min, the H component decreases from quiet time values for most events, indicating that several local substorms occurred. Note that H component began increasing at the start time, indicating that formation of the large-scale finger-like structures occurs at the beginning of the substorm recovery phase. As for the Z component, the magnetogram decreases close to the start time, indicating that Tromsø is at latitudes

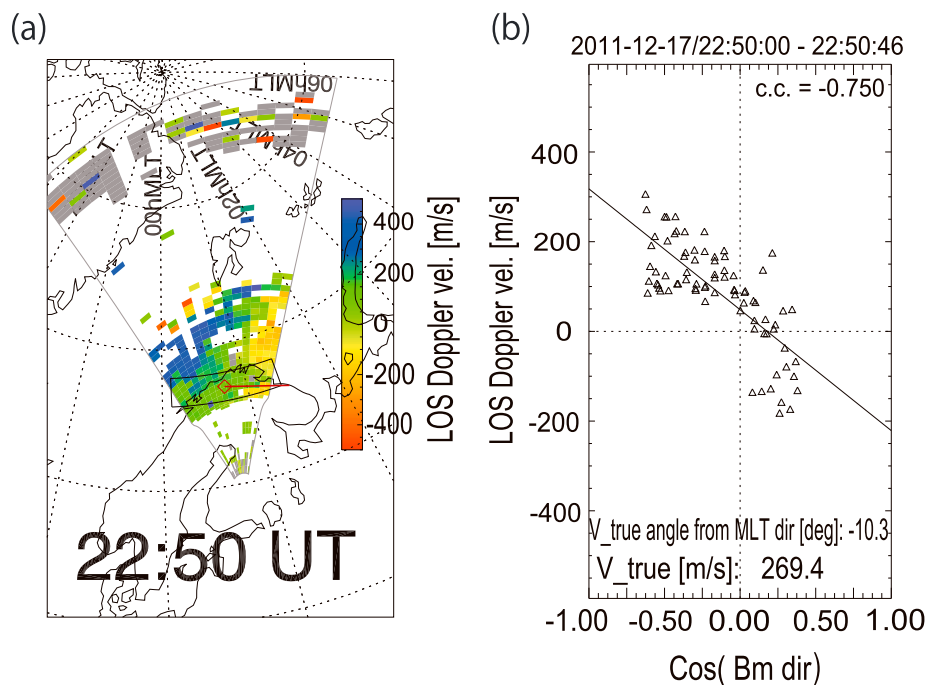


Figure 10. (a) A Doppler velocity map obtained from the SuperDARN Hankasalmi radar at 22:50 UT on 17 December 2011. The blue and red colors, respectively, indicate plasma flow toward and away from the radar. (b) The relation between the east-west beam angle from the meridional plane and line-of-sight Doppler velocity within the area shown by zonal square in Figure 10a.

lower than the main latitude of the westward electrojet current. No noteworthy characteristics are seen in the E component panel.

Figure 9 shows magnetograms for Tromsø at the time when the small-scale finger-like structures were observed in the same format as Figure 8. The H component decreased approximately 650 min before the start time, indicating that a local substorm happened. The H component is recovering from negative to positive values at the start time, indicating that the small-scale finger-like structures formed in the late recovery phase of the substorm. No remarkable characteristics are seen in the other panels.

4. SuperDARN Radar

Figure 10a shows a Doppler velocity map obtained on 17 December 2011 from the SuperDARN radar located in Hankasalmi, Finland. Blue and red indicate that the line-of-sight velocity measured by the SuperDARN radar is toward (positive value) or away from (negative value) the radar, respectively. In this figure, the velocity in the left half of the radar field of view is toward the radar, while the velocity in the right half is away from the radar. These observations are consistent with an eastward plasma flow in this region at the observed time. To determine the eastward plasma velocity, we investigated the relation between line-of-sight velocities and beam directions. Figure 10b shows the correlation between the cosine of the beam directions and the line-of-sight Doppler velocity within the zonal square in Figure 10a. We used a method similar to the one used by *Makarevich and Dyson* [2007], assuming a uniform east-west flow at magnetic latitudes of 66° – 68° . There are 76 data points in this plot, and the correlation coefficient was 0.750. We then fitted a straight line to this scattered plot and from the slope of this line obtained an eastward velocity of 269 m/s.

Table 1 presents a comparison of the eastward propagation velocity for auroras, as determined from the keograms in Figures 4 and 5, and the eastward plasma drift velocity in the ionosphere, as derived from the SuperDARN radar data and shown in the example in Figure 10b. The criteria for choosing SuperDARN data were (1) the number of data points exceeded 50, (2) the correlation coefficient between the cosine of beam direction and the line-of-sight velocity exceeded 0.7, and (3) data were recorded in both the east and west sides of the radar's field of view. By using these criteria, we determined the drift velocities for four large-scale and one small-scale finger-like structure: Eastward velocities of large-scale structures were approximately

Table 1. Comparison Between Plasma Drift Velocity and Auroral Propagation Velocity^a

	Large-Scale Finger-Like Structures			Small Scale	
	2011/11/5	2011/12/17	2012/1/29	2012/11/17	2012/1/25
Latitude (°N)	66–68	66–68	66–68	67–70	66–70
Time (UT)	0310, 0320, 0330, 0340	2240, 2250	0410, 0430, 0440	0450, 0510	0450, 0500
Auroral propagation velocity (m/s)	151	204	63	109	-44
Plasma drift velocity (SuperDARN) (m/s)	186 ± 50	311 ± 42	115 ± 26	122 ± 14	-151 ± 33
(Auroral velocity) – (plasma velocity) (m/s)	-34	-108	-52	-13	107
(Plasma velocity)/ (auroral velocity)	1.2	1.5	1.8	1.1	3.5

^aPositive: eastward.

110–310 m/s, and westward velocities of small-scale structures were approximately 150 m/s. These auroral velocities correspond to the slowest part of the typical longitudinal auroral velocities during nighttime (e.g., 50–2000 m/s in Nakamura and Oguti [1987]). The auroral velocities are comparable (within a factor of 2) to the plasma drift speeds observed by the SuperDARN radar.

The source ion energies may be estimated by considering the negative difference (–13 to –108 m/s) between the plasma and auroral velocities; these represent the curvature and gradient *B* drift velocity of protons. The estimated proton energies were 0.1–1.2 keV under the assumption of a dipole field at *L* = 6.6 Re. However, this difference in velocities is comparable with the uncertainty in velocity determination from the keogram (20–50 m/s). Gillies *et al.* [2009] showed that velocities calculated by the SuperDARN radar can become slightly faster with accounting for the refractive index of the ionosphere, which may raise the estimate of the ion energies.

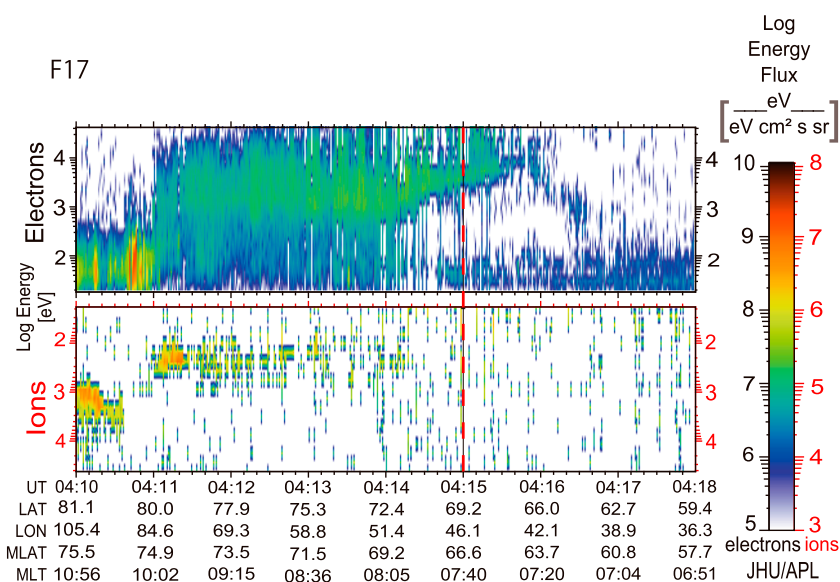


Figure 11. Electron and ion energy spectra observed by the DMSP-17 satellite at the time around the auroral fragmentation on 21 January 2012. The DMSP satellite was located about 1900 km east of Tromsø at 0415 UT. The red line indicates the latitude where the auroral fragmentation was observed.

5. DMSP Satellite

We also investigated precipitating electron and ion spectra observed by the DMSP satellite near the auroral fragmentation region. Figure 11 shows electron and ion spectra observed by the DMSP-F17 satellite around the auroral fragmentation on 21 January 2012. This is the closest location among all DMSP satellite data analyzed during the present events, approximately 1900 km east of Tromsø at 0415 UT. The red line indicates the latitude where auroral fragmentation was observed. We found that auroral fragmentation occurred near the low-latitude boundary of precipitating plasma sheet electrons at energies of a few to 10 keV. Ion precipitation was not observed in this latitude region. This may be because the plasma sheet ion energy exceeded the upper energy limit (30 keV) of the ion detector or because the flux of precipitating ions was below the sensitivity of the ion detector. Moreover, high-energy ions do not enter the dawn sector, because strong magnetic drift in the inner magnetosphere prevents this.

6. Discussion

We performed a statistical analysis of 14 large-scale and 6 small-scale finger-like structures using data from auroral observations made during a time frame of about three winters. The occurrence rate was 17.6% (41.5 out of 235.5 h of all the zenith auroral observations), suggesting that auroral fragmentation is not infrequent feature in the creation of auroral patches during substorm recovery phases. The average sizes and standard deviations of the large- and small-scale structures were 48 ± 20 km and 15 ± 5 km, respectively. The scales of these large- and small-scale structures mapped at a distance of 6.6 Re in the magnetosphere (assuming a dipole field) were 809 ± 339 km and 256 ± 85 km, respectively. These values indicate that MHD instabilities probably caused the observed auroral fragmentation, because the values are larger than the proton gyroradius in the source magnetosphere (133 km for 10 keV at 6.6 Re, $B = 110$ nT). However, the size of small-scale structures was barely twice the proton gyroradius, suggesting that the effects of finite gyroradius may come into play in the case of the small-scale finger-like structures [e.g., Hiraki and Sakaguchi, 2010].

Small-scale structures appeared when the eastward auroral speed slowed, suggesting that eastward flow suppresses the instability. The large-scale structures propagated to the east, probably because of ordinary plasma convection. Due to magnetic curvature and gradient at midnight, propagation speeds of the aurora are much slower than the typical speed for 10 keV electron drift (~ 900 m/s) and are comparable with the ionospheric plasma drift observed by SuperDARN in all but one case.

The auroral images and data from the DMSP satellite indicate that almost all of the large-scale structures occurred near the low-latitude boundary of the precipitation region of auroral particles. Given the mapping of the magnetic field line, pressure-driven instability is expected to exist in the inner part of the plasma sheet.

The large-scale finger-like structures tend to develop at the start of the substorm recovery phase, when the magnetic field structure of the magnetosphere becomes more dipole like, and so global reconfiguration of the magnetosphere might initiate the MHD instability. Small-scale finger-like structures were seen at the end of the substorm recovery phase mainly because they occur in auroral patches, which appear during the recovery phase. In addition, IMF B_z tends to turn northward at the appearance of small-scale structures, also indicating that the instabilities are initiated when the magnetic field becomes dipole like.

7. Summary

Within an observation period of about three winter seasons from January 2009 to November 2012, we found 14 large-scale and 6 small-scale finger-like structures in all-sky auroral images taken at Tromsø. We defined large-scale finger-like structures as those developing from large-scale auroral regions including arcs. The small-scale finger-like structures were defined as those developing into or out of individual auroral patches. The results obtained by the present study are summarized as follows.

1. The occurrence rates of large- and small-scale finger-like structures were 13% (31.5 h) and 4% (10 h), respectively, out of 235.5 h of zenith auroral observations. This suggests that auroral fragmentation is a common feature involved in the creation of auroral patches during the substorm recovery phase.
2. The scales of the large-scale finger-like structures were larger than the proton gyroradius in the source magnetosphere, suggesting that MHD instability is the cause of these structures. For the small-scale structures, the scales were only twice those of the proton gyroradius in the magnetosphere, suggesting that finite Larmor radius effects may also affect the creation of small-scale structures.

3. Large-scale finger-like structures appeared between midnight and dawn. Their eastward propagation speeds were among the slowest part of typical auroral drift speeds at night and were almost equal to the plasma drift speed observed simultaneously by the SuperDARN radar. Small-scale finger-like structures appeared close to dawn when the eastward drift slowed, suggesting that eastward plasma drift suppressed the instability.
4. The IMF B_z tended to be southward when large-scale finger-like structures started to develop and tended to turn northward near the start time of the small-scale finger-like structures. The AL index indicates westward electrojet current development when the large-scale structure appeared.
5. Almost all of the large-scale finger-like structures occurred near the low-latitude boundary of the auroral precipitation region, indicating that pressure-driven instability exists in the inner part of the plasma sheet.
6. Large-scale finger-like structures tended to occur at the beginning of the substorm recovery phase, suggesting that changes in the magnetic field configuration can affect the generation of these structures. Small-scale finger-like structures appeared near the end of the substorm recovery phase, mainly because they occur in auroral patches.

These results indicate that dynamic variations of the near-Earth plasma sheet, occurring at the beginning and throughout the substorm recovery phase, are capable of creating large- and small- scale pressure-driven instabilities. These instabilities are in turn responsible of causing the finger-like structures and auroral patches in the postmidnight local time sector.

Acknowledgments

We thank Y. Katoh, H. Hamaguchi, Y. Yamamoto, and T. Kawabata of the Solar-Terrestrial Environment Laboratory (STEL) at Nagoya University for their skillful support of the observations at Tromsø. OMNI data were obtained from the GSFC/SPDF OMNIWeb interface at <http://omniweb.gsfc.nasa.gov>. Solar wind and IMF data were obtained by the ACE satellite. The SYM-H, AU, and AL indices were provided by WDC-C2 for Geomagnetism at Kyoto University. The all-sky auroral images at Tromsø were provided by STEL and the National Institute of Polar Research. The DMSP particle detectors were designed by Dave Hardy of AFRL, and data were obtained from JHU/APL. A part of the work by T.H. was done at ERG-Science Center (ERG-SC) operated by ISAS/JAXA and STEL/Nagoya University. This work was supported by grants in aid for Scientific Research (20244080, 23403009, 24540478, and 25247080) from the Japan Society for the Promotion of Science and by the IUGONET Project of the Ministry of Education, Culture, Sports, Science and Technology of Japan. M.L. was supported by NERC grant NE/K011766/1.

M. Balikhin thanks two anonymous reviewers for their assistance in evaluating this paper.

References

- Chisham, G., et al. (2007), A decade of the Super Dual Auroral Radar Network (SuperDARN): Scientific achievements, new techniques and future directions, *Surv. Geophys.*, 28, 33–109, doi:10.1007/s10712-007-9017-8.
- Davis, T. N. (1978), Observed characteristics of auroral forms, *Space Sci. Rev.*, 22(1), 77–113.
- Gillies, R. G., G. C. Hussey, G. J. Sofko, K. A. McWilliams, R. A. D. Fiori, P. Ponomarenko, and J.-P. St.-Maurice (2009), Improvement of SuperDARN velocity measurements by estimating the index of refraction in the scattering region using interferometry, *J. Geophys. Res.*, 114, A07305, doi:10.1029/2008JA013967.
- Hiraki, Y., and K. Sakaguchi (2010), Formation of fingerlike structures in fragmentation of small-scale patchy aurora, *J. Geophys. Res.*, 115, A12253, doi:10.1029/2010JA015623.
- Makarevich, R. A., and P. L. Dyson (2007), Dual HF radar study of the subauroral polarization stream, *Ann. Geophys.*, 25, 2579–2591, doi:10.5194/angeo-25-2579-2007.
- Nakamura, R., and T. Oguti (1987), Drifts of auroral structures and magnetospheric electric fields, *J. Geophys. Res.*, 92, 11,241–11,247.
- Shiokawa, K., Y. Katoh, M. Satoh, M. K. Ejiri, T. Ogawa, T. Nakamura, T. Tsuda, and R. H. Wiens (1999), Development of optical mesosphere thermosphere imagers (OMTI), *Earth Planets Space*, 51, 887–896.
- Shiokawa, K., Y. Otsuka, and T. Ogawa (2009), Propagation characteristics of nighttime mesospheric and thermospheric waves observed by optical mesosphere thermosphere imagers at middle and low latitudes, *Earth Planets Space*, 61, 479–491.
- Shiokawa, K., A. Nakajima, A. Ieda, K. Sakaguchi, R. Nomura, T. Aslaksen, M. Greffen, and E. Donovan (2010), Rayleigh-Taylor type instability in auroral patches, *J. Geophys. Res.*, 115, A02211, doi:10.1029/2009JA014273.
- Shiokawa, K., et al. (2014), Auroral fragmentation into patches, *J. Geophys. Res. Space Physics*, 119, 8249–8261, doi:10.1002/2014JA020050.